

New Magnetic Fe Oxide-Carbon Based Acid Catalyst Prepared from Bio-Oil for Esterification Reactions

Fabiane C. Ballotin,^a Vitor F. Almeida,^a José D. Ardisson,^b Márcio J. da Silva,^c
Ricardo R. Soares,^d Ana Paula C. Teixeira^d* and Rochel M. Lago^a

^aDepartamento de Química, Universidade Federal de Minas Gerais, 31270-901 Belo Horizonte-MG, Brazil

^bCentro de Desenvolvimento da Tecnologia Nuclear, 31270-901 Belo Horizonte-MG, Brazil

^cDepartamento de Química, Universidade Federal de Viçosa, 36570-900 Viçosa-MG, Brazil

^dFaculdade de Engenharia Química, Universidade Federal de Uberlândia, 38408-100 Uberlândia-MG, Brazil

In this work, bio-oil (an organic matrix rich in oxygen functionalities) was used to efficiently dissolve and disperse Fe³⁺ which upon thermal treatment produced a carbon containing dispersed and encapsulated Fe oxide magnetic nanoparticles. These materials were prepared by dissolution of 8, 16 and 24 wt.% Fe³⁺ salt in bio-oil followed by treatment at 400, 450, 500 or 600 °C in N₂ atmosphere. X-ray diffraction (XRD), scanning (SEM) and transmission electron microscopies (TEM), elemental analysis, thermogravimetric-mass spectrometry (TG-MS), potentiometric titration, Raman and Mössbauer spectroscopies showed that Fe³⁺ species in bio-oil is reduced to produce magnetic nanoparticles phases: magnetite Fe₃O₄ and maghemite γ-Fe₂O₃. At low temperatures, the iron phases were less protected, and the carbon matrix was more reactive, while in temperatures above 500 °C, the iron phases were more stable, however, the carbon matrix was less reactive. Reaction of these magnetic carbon materials with concentrated H₂SO₄ produced surface sulfonic acidic sites (ca. 1 mmol g⁻¹), especially for the materials obtained at 400 and 450 °C. The materials were used as catalysts on esterification reaction of oleic acid with methanol at 100 °C and conversions of 90% were reached, however, after 2 consecutive uses, the conversion decreased to 30%, being required more studies to improve the material stability.

Keywords: bio-oil, Fe³⁺ dissolution, magnetic carbons, sulfonation, acid catalyst, esterification

Introduction

Bio-oil is a renewable and low-cost feedstock, which is generated by biomass flash pyrolysis.^{1,2} It is composed by water, alcohols, furans, acids, ketones, carbohydrates,³ and usually have highly oxygenated large carbon structures.^{4,5} These oxygen groups are considered undesirable since they bring some properties such as acidity, corrosion and thermal instability.⁶ Different upgrade processes such as cracking,⁷ decarboxylation,⁸ decarbonylation,⁹ hydrodeoxygenation¹⁰ have been investigated to decrease the oxygen content to convert bio-oil into fuel,¹¹ adhesives¹² and chemicals.¹³

On the other hand, very few studies¹⁴⁻¹⁶ have taken advantage of the oxygen and acidic properties of bio-oil. For example, the acidic characteristics of the aqueous fraction of bio-oil was used to extract iron from mining tailings to

produce different materials and fuels¹⁴ and derivatization of esterification reactions.¹⁵ The reactivity of the oxygen groups of bio-oil have also been used to produce carbon nanostructures such as graphene, nongraphite, nanotubes and nanoparticles by the simple reaction with H₂SO₄.¹⁶

In this work, bio-oil structural oxygen acidic groups were used to disperse Fe³⁺ ions. Upon thermal decomposition at different temperatures, 400-600 °C, Fe³⁺/bio-oil solution produces a carbon containing Fe oxides magnetic nanoparticles due to the carbonization and reduction of highly dispersed Fe³⁺ species. These magnetic carbon materials can have several applications in different areas such as catalysis,¹⁷⁻¹⁹ adsorption,²⁰ drug delivery,²¹ hyperthermic materials.²²

It is also described the sulfonation of these carbons, which showed reactivity dependent of thermal treatment temperature to produce magnetic acid materials which have potential application in acid-catalyzed reactions.²³ They can be used in hydrogenation,²⁴ photocatalysis,²⁵

*e-mail: anapct@ufmg.br

electrocatalysis,²⁶ dehydration and dehydrogenation of alcohols²⁷ and esterification reactions.²⁸

The catalytic esterification of fatty acids was also evaluated using sulfonated carbon based on bio-oil, once this reaction is an important alternative to convert acid vegetable oils into biodiesel. Sulfuric acid has been used as homogeneous catalyst,²⁹ however, corrosion problems and loss of the catalyst have been considered important drawbacks.^{30,31}

Therefore, the sulfonation process of carbon materials to develop heterogeneous catalysts to produce biodiesel using acidic oils is of considerable importance.^{32,33} Biomass incomplete carbonization and sulfonation has been done to produce acid catalyst. In literature, it was found that corn straw,²⁹ glucose³⁰ and starch of mung bean,³¹ were used as carbon source to produce sulfonated carbon materials with 2.64, 1.0 and 1.53 mol g⁻¹ of acidity which were used as acid catalysts on esterification reactions.

Thus, in this work, a novel application of bio-oil to produce an efficient acidic and magnetic carbon-based catalysts was investigated.

Experimental

Bio-oil production

Bio-oil was obtained in a plant at Federal University of Uberlândia, MG, Brazil, from pyrolysis of sugarcane straw at 450 °C. It is composed of carbohydrates, phenols, furans, guaiacols, syringols and presented 46% C and 7% of H.¹⁶

Iron impregnation

Bio-oil (5.0138 g) was dissolved in 20 mL of ethanol and impregnated with an ethanolic solution of 8, 16 and 24 wt.% Fe, Fe(NO₃)₃·9H₂O.^{34,35} The solution remained under stirring for 30 min. After this time, the solvent was evaporated and the solid obtained were dried for 12 h at 353 K. The dried sample were named here as B8Fe, B16Fe or B24Fe, respective to the Fe percentage.

Pyrolysis

About 800 mg of B8Fe were thermally treated in a tubular oven at 400, 450, 500 and 600 °C for 1 h in N₂ atmosphere (50 mL min⁻¹).^{34,35} The obtained materials were named hereon as (B8Fe)₄₀₀, (B8Fe)₄₅₀, (B8Fe)₅₀₀ and (B8Fe)₆₀₀, respective to the thermal treatment temperature.

Sulfonation

0.5000 mg of the pyrolyzed sample was submitted to a sulfonation reaction with a ratio 9.2:1 m/m of concentrated H₂SO₄:bio-oil at 120 °C for 2 h, under magnetic stirring.^{28,36} After the reaction, the materials were washed with distilled water until pH ca. 5.50 and dried at 80 °C for 12 h. The catalyst yield was calculated according to equation 1:

$$\text{Yield}(\%) = (w_{\text{final}} / w_{\text{initial}}) \times 100 \quad (1)$$

where w_{initial} is the material weight before thermal treatment and w_{final} is the weight after pyrolysis and sulfonation process.

The catalysts were named as (B8Fe)₄₀₀S, where S refers to sulfuric acid treatment.

Materials characterization

The content of some elements (carbon, hydrogen, nitrogen and sulfur) on the synthesized materials was determined by elemental analysis using PerkinElmer CHN analyzer. Scanning electron microscopy (SEM) images were obtained in a FIB, Quanta FEG 3D FEI equipment. The samples were dispersed in acetone and deposited onto a silicon plate. The transmission electron microscopy (TEM) images were obtained in a G2-20, SuperTwin FEI, 200 kV.

X-ray diffraction (XRD) studies were performed on a Shimadzu diffractometer, model XRD-7000 with Cu K α and a scan speed of 4° min⁻¹. Thermogravimetric analysis (TGA) was performed on a Shimadzu DTG 60H with air flow (50 mL min⁻¹) and a heating rate of 10 K min⁻¹ up to 1273 K. Catalyst acidity was measured by potentiometric titration. The solid (0.05 g) were suspended in acetonitrile (40 mL) and shaken for 24 h. Then, the suspension was potentiometrically titrated with a 0.025 mol L⁻¹ *n*-butylamine solution in toluene. The electrode potential variation was measured with a BEL pH instrument.

Simultaneous thermogravimetric-mass spectrometry (TG-MS) analyses were performed. The base peaks (m/z 18, 28, 44, 64 and 80) were selected to be monitored in a NETZSCH TG/STA equipment coupled with Aelos spectrometer, model 7.0. The samples specific surface areas were analyzed by adsorption of N₂ at 77 K using analyzer Quantachrome, model NOVA 1200e. The samples were degassed at 80 °C for 4 h before the analyses. The absorption spectroscopy measurements in the infrared region with Fourier transform (FTIR) attenuated total reflectance (ATR) were performed on PerkinElmer equipment, model Spectrum 1000. Spectra were collected in the range of 400-4000 cm⁻¹ region, with 64 accumulations.

Raman spectra of carbon material obtained from bio-oil were acquired using Raman Senterra spectrometer, 532 nm laser line was used for excitation with the exposure time of 60 s and 10 mW of power.

^{57}Fe Mössbauer spectra (MS) were obtained at room temperature and at 30 K, in transmission geometry with a source of ^{57}Co in Rh matrix. Spectral hyperfine parameters were calculated using the Normos least-squares-fit software package.³²

Catalytic runs

The esterification reactions of oleic acid with methanol were performed in a sealed tube glass reactor with sampling septum in a thermostatic bath with magnetic stirring. Dodecane was used as internal standard. The solid catalysts, i.e., $(\text{B8Fe})_{400}\text{S}$, $(\text{B8Fe})_{450}\text{S}$, $(\text{B8Fe})_{500}\text{S}$ and $(\text{B8Fe})_{600}\text{S}$, were used in variable loads (ca. 1-10 wt.%). The reactions were performed at temperature ranging of 60-100 °C.³⁷ The oleic acid:methanol molar ratio used was 1:30³⁸ (0.58 mL of oleic acid and 2.22 mL of methanol).

Catalyst reuse

The reuse test was performed using 10 wt.% of catalyst $(\text{B8Fe})_{450}\text{S}$, 1:30 oleic acid:methanol, at 100 °C during 6 h. After each reaction, the catalyst was separated from the products using a magnet, washed with methanol and reuse reactions were performed.

Catalyst leaching

Leaching was evaluated at the oleic acid:methanol molar ratio of 1:30, using 10 wt.% of catalyst $(\text{B8Fe})_{450}\text{S}$. For the tests, the catalyst was transferred to the reaction medium containing only methanol. The system was maintained under constant stirring for 90 min at 100 °C. After this period, methanol was removed and transferred to a vial containing only oleic acid, thus proceeding with the reaction.

Analysis of products

After the reaction, the mixture was dissolved in 3 mL of hexane. The methyl ester was quantified in a gas chromatography coupled with flame ionization detector (GC-FID) using a Shimadzu GC-2010, equipped with a Carbowax capillary column (0.25 m × 0.25 mm × 30 m).

Results and Discussion

Previous GC-MS and ^1H nuclear magnetic resonance

(NMR) characterization of bio-oil showed a complex matrix composed of syringols, phenols, carboxylic acids, aldehydes, ketones, alcohols and a heavier fraction containing oligomers with different oxygen functionalities.¹⁶ FTIR and elemental analyses confirmed the presence of a great amount of oxygen groups, ca. 48% (Figure 1).

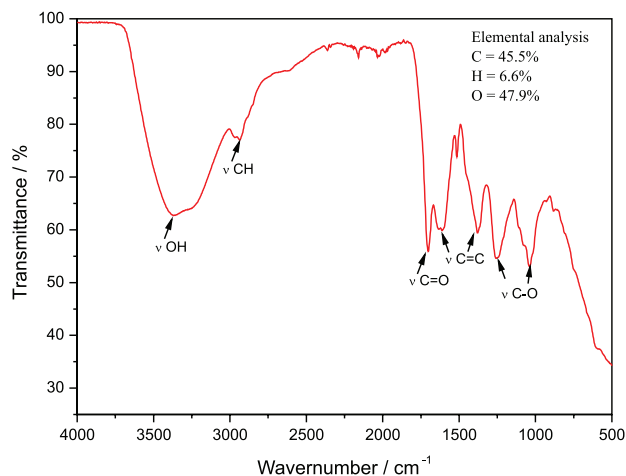


Figure 1. Infrared spectrum (ATR) and elemental analysis of bio-oil (adapted from reference 16).

It is interesting to observe that $\text{Fe}(\text{NO}_3)_3$ could be well solubilized in rather hydrophobic organic matrix bio-oil. Although the mechanism responsible for this solubilization of Fe^{3+} is not clear, the interaction/complexation with different oxygen groups such as phenolic and carboxylic is most likely involved in this process.

Three different bio-oil solutions in ethanol were prepared containing 8, 16 and 24 wt.% $\text{Fe}(\text{NO}_3)_3$ (in relation to bio-oil content). After 30 min of stirring, the solvent was evaporated to produce a viscous/vitreous precursor. No visual indication that $\text{Fe}(\text{NO}_3)_3$ was crystallized, segregated or separated from the bio-oil was observed. The precursors were thermally treated in nitrogen atmosphere at 450 °C for 1 h.

XRD analyses of the obtained materials (Figure S1, Supplementary Information (SI) section) showed the formation of magnetic iron phases, e.g., magnetite (Fe_3O_4)/maghemite ($\gamma\text{-Fe}_2\text{O}_3$). The samples were sulfonated with H_2SO_4 and tested as catalysts in oleic acid esterification reactions. The tests showed that when materials $(\text{B16Fe})_{450}\text{S}$ and $(\text{B24Fe})_{450}\text{S}$ were used, a large amount of iron oxide was leached, and no formation of biodiesel occurred. Probably, in these samples, the carbon was not sufficient to protect the iron phases.

Therefore, the effect of thermal treatment was investigated in more detail for the sample B8Fe which was treated at 400, 450, 500 and 600 °C. In general, the samples presented low crystallinity as showed by XRD (Figure S2,

SI section), with two peaks observed for all samples at ca. 24° related to the amorphous carbon³³ and 35° , likely related to Fe_3O_4 (magnetite) (JCPDS1-1111) or $\gamma\text{-Fe}_2\text{O}_3$ (maghemite) (JCPDS:39-1346).³⁹

After sulfonation (Figure 2), a broad peak at 24° was observed for sample $(\text{B8Fe})_{400}\text{S}$. However, the peak related to iron phase disappeared, due to iron leaching in the presence of H_2SO_4 .

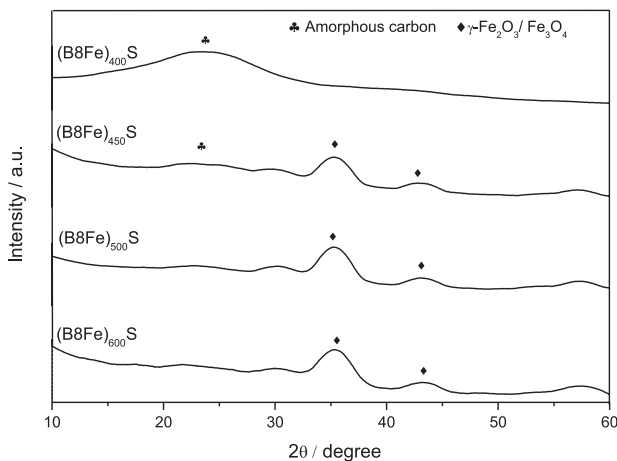


Figure 2. XRD patterns of samples $(\text{B8Fe})_{400}\text{S}$, $(\text{B8Fe})_{450}\text{S}$, $(\text{B8Fe})_{500}\text{S}$ and $(\text{B8Fe})_{600}\text{S}$.

As the temperature of treatment increased, the iron phase became more structured and the peaks at 35 and 43° related to Fe_3O_4 (magnetite) or $\gamma\text{-Fe}_2\text{O}_3$ (maghemite) were observed. Scherrer equation was used to estimate the crystallite size of the iron oxide which was in the range of 3-5 nm.

Mössbauer spectra before (Figure S3, SI section) and after sulfonation (Figure 3), consisted of a set of six-lines pattern related to a ferromagnetic material indicating a mixture of maghemite/magnetite (hyperfine parameters are shown in Table S1, SI section). According to measurements, the samples at room temperature presented a superparamagnetic behavior. At 30 K, $(\text{B8Fe})_{450}$ and $(\text{B8Fe})_{450}\text{S}$ still present superparamagnetic character, however, as temperature of thermal treatment increased, the samples presented a higher degree of organization.

According to XRD and Mössbauer results, after bio-oil impregnation with $\text{Fe}(\text{NO}_3)_3$ and thermal treatment ($400\text{-}600^\circ\text{C}$) under N_2 atmosphere, occurred the partial reduction of Fe^{3+} leading to the formation of a $\text{Fe}^{2+}/\text{Fe}^{3+}$ oxide. Although the mechanism for this reduction is not clear, it is most likely that reducing species such as H_2 , CO , organics and amorphous carbon formed during bio-oil decomposition⁴⁰ are involved in Fe^{3+} reduction.

SEM analyses of material treated at 400°C (Figure 4) showed that before sulfonation, the material presented particles between 50 and $300\ \mu\text{m}$. Moreover, mapping and

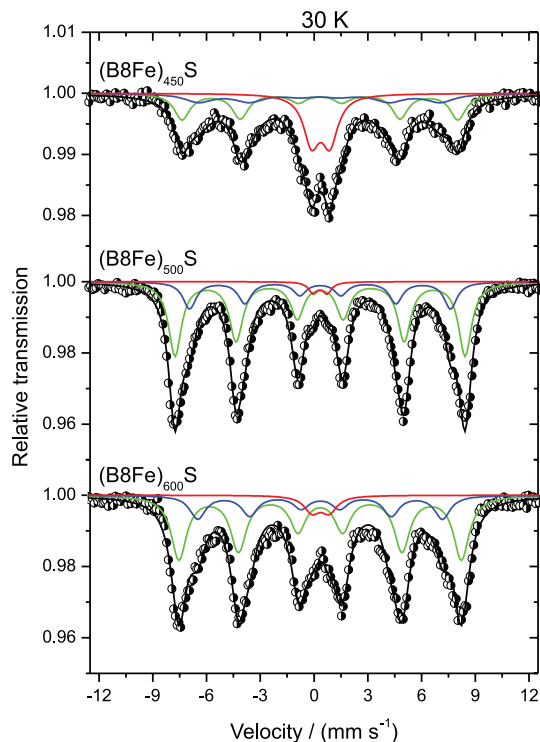


Figure 3. Mössbauer spectra at 30 K of samples $(\text{B8Fe})_{450}\text{S}$, $(\text{B8Fe})_{500}\text{S}$ and $(\text{B8Fe})_{600}\text{S}$.

energy-dispersive X-ray spectroscopy (EDS) (Figure S4, SI section) analyses showed that iron was leached by sulfuric acid indicating that the carbon formed did not encapsulate/protect the Fe oxide particles.

After sulfonation (Figure 4), particles of $50\ \mu\text{m}$ and irregular surfaces were observed.

TEM images for material treated at 400°C and sulfonated showed no iron in its structure confirming acid leaching (Figure S5, SI section). For samples treated at temperatures 450, 500 and 600°C (Figures 5-6), iron was dispersed all over the materials surface and remained encapsulated by the carbon matrix. The images and histogram (Figure 6) showed that iron nanoparticles have sizes between 5-20 nm.

The yield of catalyst synthesis as well as the evaluation of the sulfonation process was carried out by elemental analyses. Table 1 shows C, H, N and S contents in these materials.

After pyrolysis and H_2SO_4 reaction, the materials were ground and extensively washed with deionized water until pH 6.0. In general, the materials yield decreased with pyrolysis temperature increase: 50.3, 47.3, 42.1 and 39.7% for $(\text{B8Fe})_{400}\text{S}$, $(\text{B8Fe})_{450}\text{S}$, $(\text{B8Fe})_{500}\text{S}$ and $(\text{B8Fe})_{600}\text{S}$, respectively. Indeed, at higher temperatures more volatiles were released from the organic matrix.

The original bio-oil (before thermal treatment and sulfonation) presented 45.5, 6.6 and 0.5% of C, H and

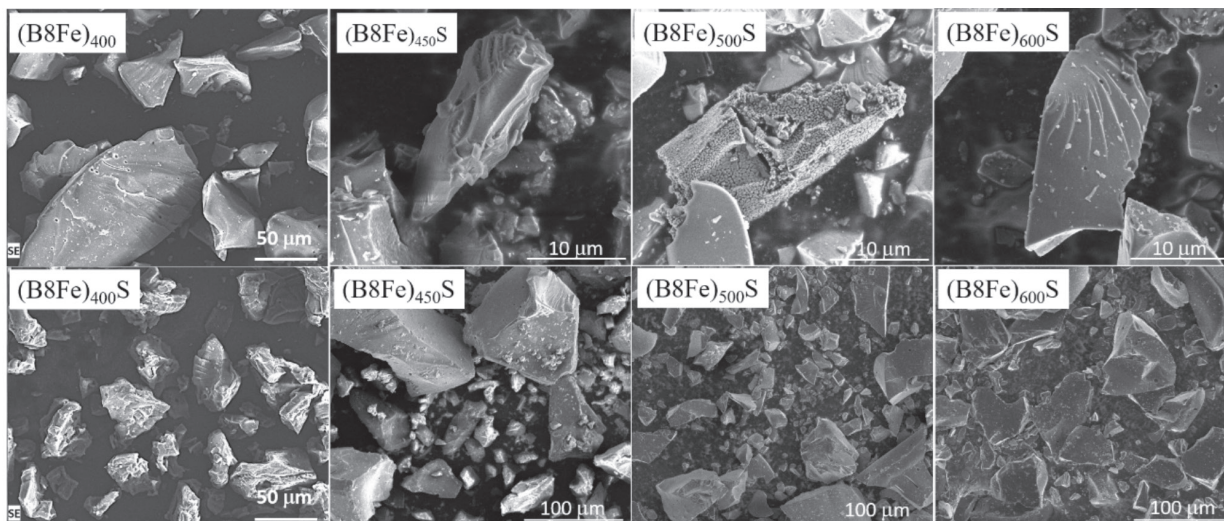


Figure 4. Scanning electron microscopy images of iron materials before, $(\text{B8Fe})_{400}$, and after sulfonation $(\text{B8Fe})_{400}\text{S}$, $(\text{B8Fe})_{450}\text{S}$, $(\text{B8Fe})_{500}\text{S}$ and $(\text{B8Fe})_{600}\text{S}$.

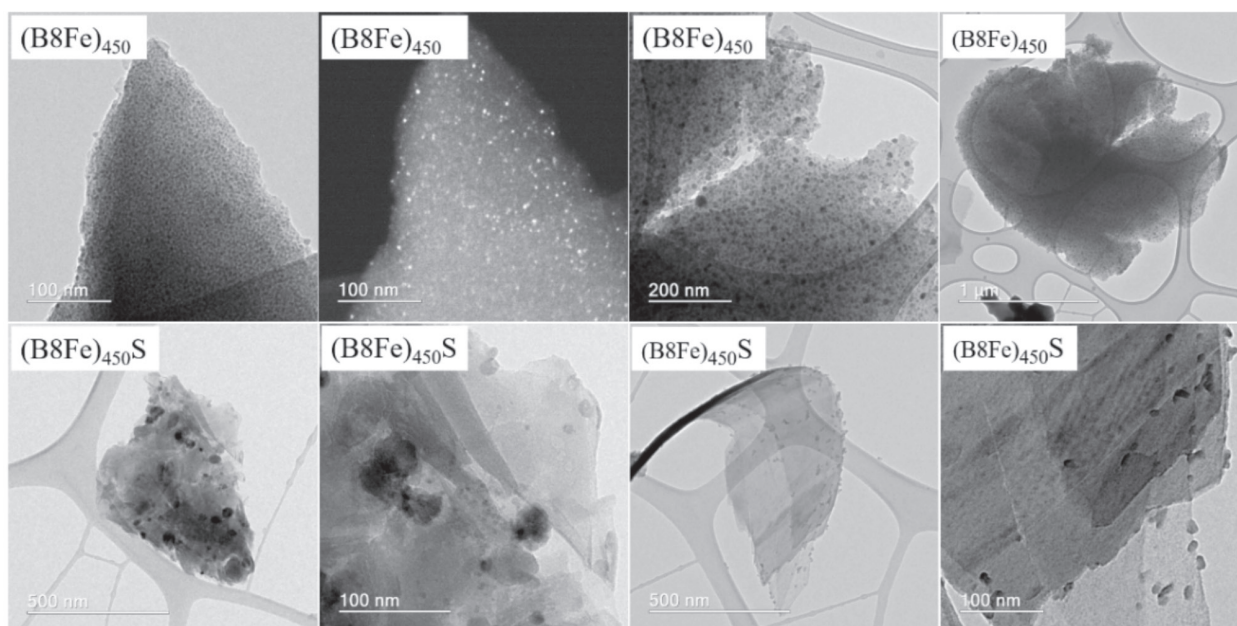


Figure 5. Transmission electron microscopy images of materials $(\text{B8Fe})_{450}$ and $(\text{B8Fe})_{450}\text{S}$.

N,¹⁶ respectively. According to elemental analysis, carbon content increased from ca. 46 to 48-54% and the H content decreased for sample $(\text{B8Fe})_{400}\text{S}$, due to dehydration and carbonization. Furthermore, the presence of 3.4-4.5% N indicates the presence of non-decomposed nitrate and likely nitrogen groups formed during the process.

Relatively high sulfur content was observed, i.e., 5.0%, for the sample $(\text{B8Fe})_{400}\text{S}$ likely due to the sulfonation of the carbon formed after treatment at 400 °C. On the other hand, S decreased to 3.8, 2.5 and 2.2% as the material was pre-treated at 450, 500 and 600 °C, respectively. This result suggests that thermal treatment at temperatures higher than 400 °C is producing carbons that are well structured and more difficult to sulfonate.

Raman spectra of materials (Figure 7) showed two bands characteristics of carbonaceous materials,⁴¹ the G band (1590 cm^{-1}), which is related to more organized graphitic structures, and D band (1350 cm^{-1}), which indicates the presence of defects in carbonaceous structures and amorphous carbon.

The D band intensity to G band ratio (I_D/I_G) is high (approximately 0.9) for all the materials spectra, which were also verified on other studies.⁴¹ These results can be indicated that the materials have high degree of defects.

The FTIR spectra of sulfonated materials (Figure S6, SI section) showed two bands at 1583 and 1688 cm^{-1} related to aromatic C=C bonds.⁴² Furthermore, for material $(\text{B8Fe})_{400}\text{S}$ a broad band near 3026 cm^{-1} related to -OH

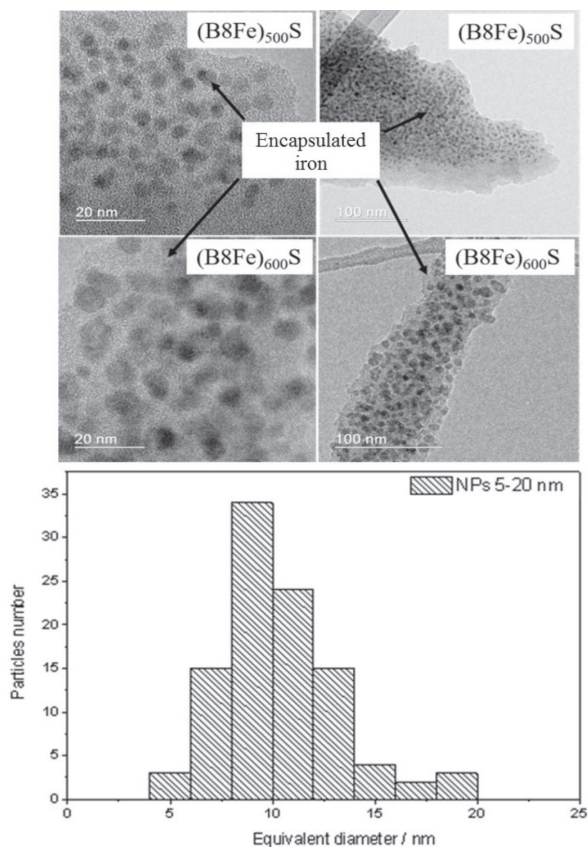


Figure 6. (Top) Transmission electron microscopy images of materials $(B8Fe)_{500}S$ and $(B8Fe)_{600}S$ and (bottom) particle size distribution.

Table 1. C, H and N content of bio-oil and materials impregnated with 8 wt.% of iron (B8Fe) and sulfonated

Sample	C / %	H / %	N / %	S / %
Bio-oil	45.5	6.6	0.5	–
$(B8Fe)_{400}S$	54.3	2.9	4.4	5.0
$(B8Fe)_{450}S$	49.0	3.1	4.5	3.8
$(B8Fe)_{500}S$	50.3	2.5	4.1	2.5
$(B8Fe)_{600}S$	48.4	1.8	3.4	2.2

$(B8Fe)_{400}S$, $(B8Fe)_{450}S$, $(B8Fe)_{500}S$, $(B8Fe)_{600}S$: bio-oil impregnated with 8 wt.% of iron, sulfonated and thermally treated at 400, 450, 500 or 600 °C, respectively.

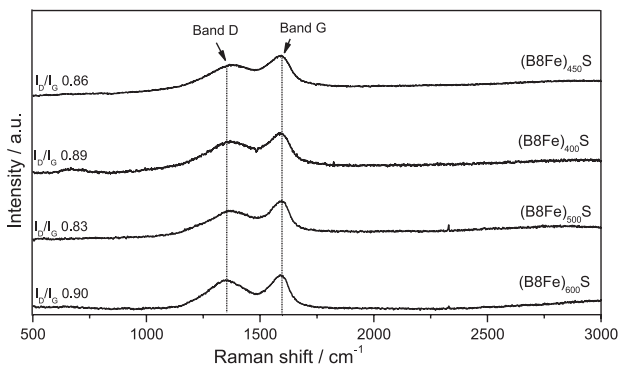


Figure 7. Raman spectra of materials $(B8Fe)_{400}S$, $(B8Fe)_{450}S$, $(B8Fe)_{500}S$ and $(B8Fe)_{600}S$.

stretching was observed. At 1143 and 1019 cm^{-1} , two bands related to the symmetric and asymmetric stretching of $\text{O}=\text{S}=\text{O}$ group indicate the presence of $-\text{SO}_3\text{H}$ groups.⁴³ At temperatures higher than 400 °C, a significant decrease on the bands intensity was observed, confirming the release of oxygenated compounds during carbonization.⁴⁴ Besides that, decrease on the intensity bands relative to sulfonic groups was also verified.⁴⁴

The TG curves in air of the sample $(B8Fe)_{400}$ showed an initial weight loss of 6% related to water, followed by 55% loss between 230–400 °C related to carbon oxidation/organics decomposition (Figure S7, SI section) leaving ca. 38% of iron oxide. On the other hand, the TG curve of the material $(B8Fe)_{400}S$ indicated a final iron oxide content of only 7% due to leaching caused by sulfuric acid treatment.

The materials $(B8Fe)_{500}$, $(B8Fe)_{500}S$, $(B8Fe)_{600}$ and $(B8Fe)_{600}S$ showed similar TG curves (Figure S8, SI section), i.e., mass losses between 300 and 430 °C, concerning the oxidation of carbonaceous structures. In all curves, about 37 to 44% of the inorganic was observed, before and after the sulfonation process. It is probably related to iron phases which are protected and covered by coal and to ashes from the coal oxidation.⁴⁵ For materials $(B8Fe)_{450}$ and $(B8Fe)_{450}S$, the weight loss began near 260 °C, indicating that materials are less stable, leading to a final weight of 30 and 25%, respectively. The higher weight loss for $(B8Fe)_{450}S$ could be related to iron leaching.

In order to analyze what occurred during material thermal decomposition, a TG-MS experiment (Figure 8) was performed monitoring the m/z signals 18, 28, 44 and 64 with materials $(B8Fe)_{450}$ and $(B8Fe)_{450}S$, in argon atmosphere. Both samples showed initial weight loss until 150 °C due to water (m/z 18). Adsorbed CO_2 was also released at ca. 100 °C. After 150 up to ca. 700 °C several signals related to CO_2 were observed probably due to the decomposition of oxygen groups present in the carbon structure. The m/z signal 28 related to CO was observed between 600–700 °C and is usually related to the decomposition of oxygen directly linked to the carbon structures.⁴⁶

It was observed that sulfonation with H_2SO_4 caused slight changes in the TG-MS desorption profiles. However, the main difference is the presence of an m/z signal 64 between 250–400 °C related to SO_2 originated from HSO_3^- surface groups.⁴⁷

The number of acid sites determined based on the total amount of sulfur indicated values of 1.56 mmol g^{-1} for the sample $(B8Fe)_{400}S$ and 1.19 mmol g^{-1} for $(B8Fe)_{450}S$. On the other hand, potentiometric titration measurements (Figure S9, SI section) suggested much lower values of

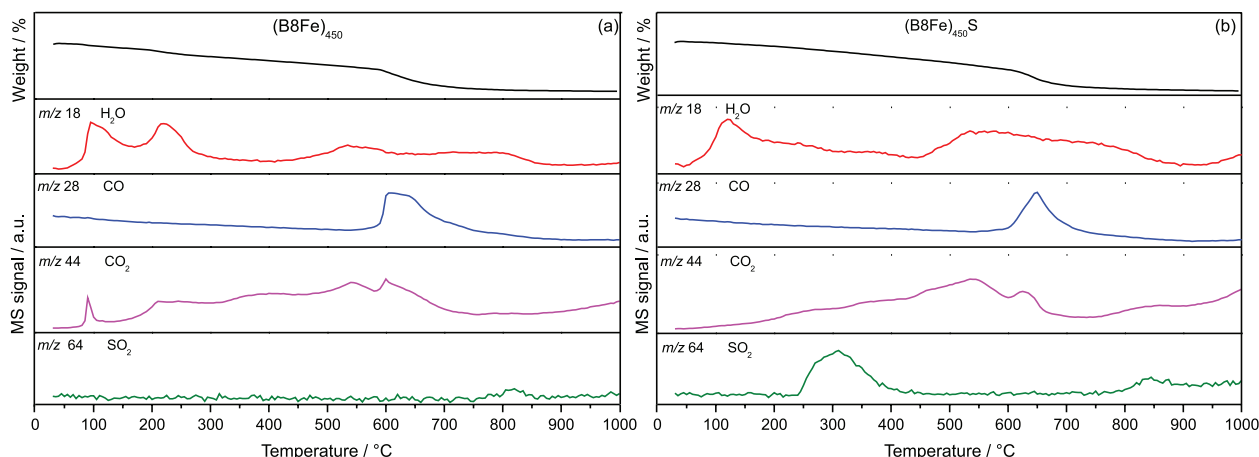


Figure 8. TG and MS curves on argon atmosphere, heating rate of $10\text{ }^{\circ}\text{C min}^{-1}$ of materials: (a) $(\text{B8Fe})_{450}$; (b) $(\text{B8Fe})_{450}\text{S}$.

ca. 0.2 mmol g^{-1} for the sample $(\text{B8Fe})_{400}\text{S}$ which strongly decreased for treatment at higher temperatures. Again, these results indicate that thermal treatments at 500 and $600\text{ }^{\circ}\text{C}$ led to the formation of a very stable carbon less susceptible to sulfonation.

Sulfonated biochar based on pine and starch presented $0.2\text{--}0.9\text{ mmol g}^{-1}$ of acid sites density.⁴⁸ However, solid catalysts based on glucose,⁴⁹ starch and cellulose,⁵⁰ presented density of acid sites higher than 1 mmol g^{-1} , which is explained by their large area, pore volume and pore size. According to studies,⁵⁰ materials with larger areas and pore size make the reactants more accessible to SO_3H groups. Studies^{46,49} showed that lower acid densities can be attributed to higher cross linking and degree of polymerization at higher temperatures, reducing sulfonation efficiency.

The materials were characterized by adsorption/desorption using Brunauer-Emmett-Teller (BET) method and the surface areas were similar, e.g., 3, 2, 2 and $3\text{ m}^2\text{ g}^{-1}$ for $(\text{B8Fe})_{400}\text{S}$, $(\text{B8Fe})_{450}\text{S}$, $(\text{B8Fe})_{500}\text{S}$ and $(\text{B8Fe})_{600}\text{S}$, respectively. These low values can be attributed to the presence of a great amount of organic compounds, which could be released at higher temperatures.⁵¹⁻⁵³

Catalytic tests

Esterification reactions of oleic acid in the presence of methanol catalyzed by the produced materials were studied (Figure 9). The use of the same quantity of catalyst, e.g., 10 wt.%, 1:30 oleic acid:methanol, for 6 h at $100\text{ }^{\circ}\text{C}$, showed different conversions. As expected, when the material $(\text{B8Fe})_{400}\text{S}$ was used, the reaction occurred rapidly, reaching the equilibrium in 2 h. The conversion after 6 h was 99%. In the other hand, when the material $(\text{B8Fe})_{450}\text{S}$ was used, the reaction gradually reached the equilibrium after 5 h, with a conversion of 90%.⁵⁴ When other materials were

assessed, $(\text{B8Fe})_{500}\text{S}$ and $(\text{B8Fe})_{600}\text{S}$, no significant catalytic effect was observed, what corroborates potentiometric titration analysis. The insignificant conversion was also observed for blank reaction and for material $(\text{B8Fe})_{450}$ (not showed).

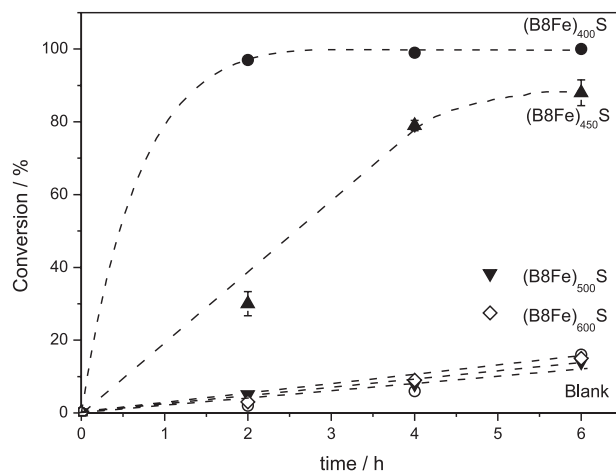


Figure 9. Oleic acid conversion versus time on esterification reaction: effect of the catalyst nature. Reaction conditions: 10 wt.% catalyst, 1:30 oleic acid:methanol, $100\text{ }^{\circ}\text{C}$.

The difference on materials catalytic activity is strictly related to pyrolysis temperature. At low temperatures ($400\text{--}450\text{ }^{\circ}\text{C}$), the materials were partially carbonized, which allowed the organic groups to react with H_2SO_4 . The rise of temperature produced a well-structured carbon which present low concentration of surface acid sites,⁴⁸ what was confirmed by CHNS and potentiometric titration. It is also important to highlight that iron played no significant role on the material acidity, once the material $(\text{B8Fe})_{450}$ showed no catalytic activity.

In fact, esterification reactions using wood-based activate carbon catalyst in similar conditions (1:10 oleic acid methanol, 10 wt.% at $100\text{ }^{\circ}\text{C}$, 3 h) had also a significant

esterification activity, being the biochars synthesized at lower temperatures the most active catalysts.⁴⁸ The more drastic conditions used in this work can be explained due to lower acid sites. In fact, herein, the materials were sulfonated for 2 h at 120 °C, while in the previous study,⁴⁸ the materials were in contact with H₂SO₄ for 12-18 h.

More detailed investigation was carried out with the magnetic catalyst (B8Fe)₄₅₀S, in which the temperature effect was studied. The temperature rises from 60 to 100 °C produced a gradual increase in the yield of esters from 56 to 90% (Figure 10). This effect is likely kinetic but also related to the higher solubility of methanol in oleic acid,⁵⁵ a high temperature often obtains satisfactory yields, as showed in a study⁵⁶ with acid magnetic catalyst, in which the yield increased from 78.9 to 98.9% when the temperature rose from 50 to 70 °C.

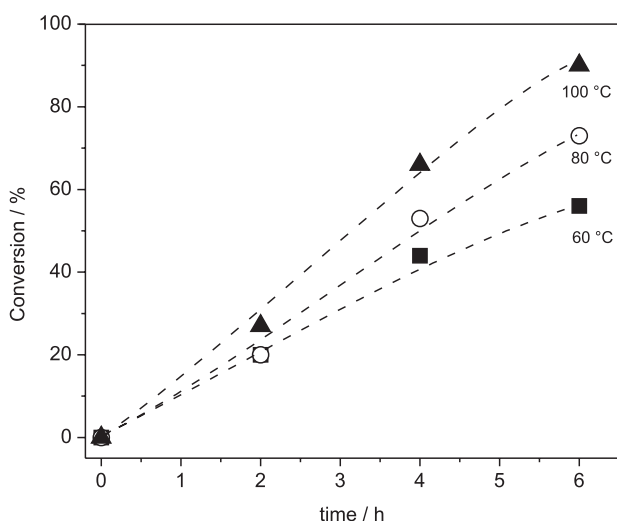


Figure 10. Oleic acid conversion *versus* time on esterification reaction: effect of the reaction temperature. Reaction conditions: 10% catalyst (B8Fe)₄₅₀S, 1:30 oleic acid:methanol, 6 h reaction, at 60, 80 and 100 °C.

After the reaction, the catalyst (B8Fe)₄₅₀S was separated from the products using a magnet, washed 2 times with methanol and reuse reactions were performed. After 2 reuses a decrease on the conversion to 30% was observed (Figure 11). Previous works^{44,45} suggested that deactivation processes are likely related to -SO₃H groups leaching and due to organic molecules, that poison the material active sites. Unlike other magnetic catalysts, which could be reused for 6 times,^{17,56} in this study the material did not present high stability, that could also be related to the synthesis method used.

In fact, leaching processes were also performed by leaving the catalyst in contact with methanol for 30 min, after that, methanol was added to a flask with oleic acid. It can be seen that about 32% of the catalyst active sites were leached to the reaction medium.

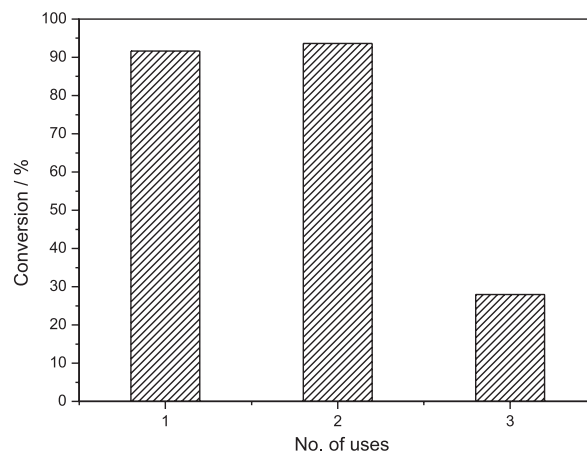
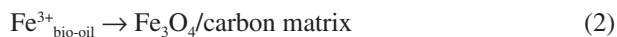


Figure 11. Oleic acid conversion *versus* number of uses on esterification reaction: recycling reactions of catalyst (B8Fe)₄₅₀S. Reaction conditions: 10.0 wt.% catalyst, 1:30 oleic acid:methanol, 100 °C, 6 h.

The catalytic tests showed that sulfonated materials were active to esterification reactions, with conversions of 90%, however, the legislation requires a conversion of > 96%. In that way, it would be necessary to increase the oleic acid:methanol ratio to move the reaction towards products formation or increase the number of acidic sites, adding more catalyst to the reaction medium.

The mechanism involves the proton of SO₃H groups, which works as a Brønsted acid. Furthermore, at temperatures higher than 450 °C, the materials were magnetic, which facilitates the material removal from reaction medium. Reuse tests of (B8Fe)₄₅₀S demonstrated that after 3 uses the conversion decreases to 30%, probably because of leaching or methylation of SO₃H. Studies³⁶ performed with a carbon based on bamboo catalyst showed that after 2 h of reaction, using 6 wt.% of catalyst, 1:5 oleic acid:ethanol at 90 °C, the conversion was 97%. However, after the 5th use, the conversion decrease to 27.84%.

The results obtained in this work, e.g., SEM, TEM, TG, Mössbauer and XRD, indicated that Fe³⁺ can be dispersed in bio-oil and upon thermal treatment at temperatures higher than 400 °C is reduced to form magnetite Fe₃O₄ nanoparticles:



During decomposition the presence of oxidizing molecules, e.g., H₂O and CO₂, or when exposed to air, part of these Fe₃O₄ nanoparticles are oxidized to another magnetic phase maghemite γ -Fe₂O₃.



These materials can be sulfonated by a simple reaction with concentrated H₂SO₄. The most efficient sulfonation

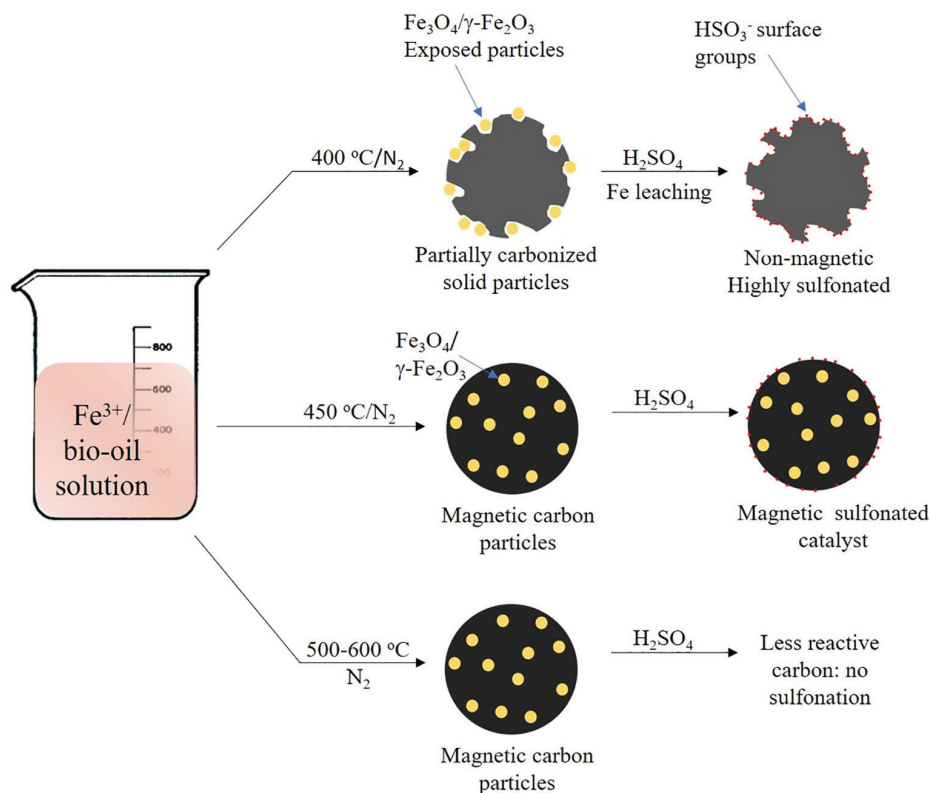


Figure 12. Scheme of carbonization and sulfonation processes of Fe^{3+} /bio-oil.

was observed for the material obtained at 400 °C. However, sulfonation of the material $(\text{B8Fe})_{400}$ led to a strong Fe leaching indicating that the metal was exposed and not encapsulated by the carbon matrix. As a result of this leaching the material was not magnetic. On the other hand, the material obtained at 450 °C, $(\text{B8Fe})_{450}$, showed good results for the sulfonation process but no significant Fe leaching suggesting that the Fe oxide particles are protected/encapsulated in the carbon matrix. Thermal treatment at 500 and 600 °C produced carbons very resistant to sulfonation. These results are summarized schematically in Figure 12.

The material $(\text{B8Fe})_{450}\text{S}$ showed good results for the esterification of oleic acid reaching 90% of conversion, similar to the most efficient catalysts described in the literature,⁵¹ however, more studies should improve the material stability in the reaction medium.

Conclusions

The organic matrix bio-oil rich in oxygen functionalities can be used to efficiently dissolve/disperse Fe^{3+} . Upon thermal treatment the bio-oil decomposition led to the formation of a carbonaceous matrix and the partial reduction of Fe^{3+} to Fe^{2+} to form magnetic nanoparticles of Fe_3O_4 and maghemite $\gamma\text{-Fe}_2\text{O}_3$. This composite based on Fe magnetic

nanoparticles dispersed/encapsulated in a carbon matrix has several potential applications in adsorption, catalysis and materials science. The effect of pyrolysis temperature was important, once as temperature increases, the material becomes less reactive due to sulfuric acid. These magnetic carbons were used as acid catalyst in different reactions, such as esterification of oleic acid and methanol, which reached 90% of conversion. Reuse reactions were also performed and after 2nd use, the conversion decreased to 30%, being necessary other studies to improve the catalyst stability in reaction medium.

Supplementary Information

Supplementary data are available free of charge at <http://jbcs.sbq.org.br> as PDF file.

Acknowledgments

The authors acknowledge the UFMG microscopy center, INCT Midas, CNPQ, CAPES and FAPEMIG.

Authors Contributions

Fabiane C. Ballotin was responsible for the conceptualization, data curation, investigation, writing

original draft, review and editing; Vitor F. Almeida for the data curation, investigation and validation; José D. Ardisson for the visualization, writing review and editing; Márcio J. da Silva for the visualization, writing original draft, review and editing; Ricardo R. Soares for the visualization, writing review and editing; Rochel M. Lago for the conceptualization, project administration, visualization, writing original draft, review and editing; Ana Paula C. Teixeira for the conceptualization, project administration, visualization, writing original draft, review and editing.

References

- Mortensen, P. M.; Grunwaldt, J.-D.; Jensen, P. A.; Knudsen, K. G.; Jensen, A. D.; *Appl. Catal., A* **2011**, *407*, 1.
- Bridgwater, A. V.; *Biomass Bioenergy* **2012**, *38*, 68.
- Mullen, C. A.; Boateng, A. A.; Goldberg, N. M.; Lima, I. M.; Laird, D. A.; Hicks, K. B.; *Biomass Bioenergy* **2010**, *34*, 67.
- Guo, X.; Zheng, Y.; Zhang, B.; Chen, J.; *Biomass Bioenergy* **2009**, *33*, 1469.
- Boateng, A.; Sadaka, S.; *J. Anal. Appl. Pyrolysis* **2012**, *95*, 38.
- Kim, J.-S.; *Bioresour. Technol.* **2015**, *178*, 90.
- Hew, K. L.; Tamidi, A. M.; Yusup, S.; Lee, K. T.; Ahmad, M. M.; *Bioresour. Technol.* **2010**, *101*, 8855.
- Khromova, S. A.; Smirnov, A. A.; Selishcheva, S. A.; Kukushkin, R. G.; Dundich, V. O.; Trusov, L. I.; Yakovlev, V. A.; *Catal. Ind.* **2013**, *5*, 260.
- Isa, K. M.; Ying, L. J.; Saad, S. S.; Kasim, F. H.; Rahim, M. A. A.; *J. Adv. Res. Fluid Mech. Therm. Sci.* **2016**, *27*, 12.
- Yang, T.; Shi, L.; Li, R.; Li, B.; Kai, X.; *Fuel Process. Technol.* **2019**, *184*, 65.
- Czernik, S.; French, R.; Feik, C.; Chornet, E.; *Ind. Eng. Chem. Res.* **2002**, *41*, 4209.
- Oldham, D. J.; Fini, E. H.; Chailleux, E.; *Constr. Build. Mater.* **2015**, *86*, 75.
- Chaiwat, W.; Gunawan, R.; Gholizadeh, M.; Li, X.; Lievens, C.; Hu, X.; Wang, Y.; Mourant, D.; Rossiter, A.; Bromly, J.; Li, C.-Z.; *Fuel* **2013**, *112*, 302.
- Mendonça, F. G.; Gomes, J. P. M.; Tristão, J. C.; Ardisson, J. D.; Soares, R. R.; Lago, R. M.; *Fuel* **2016**, *184*, 36.
- Milina, M.; Mitchell, S.; Pérez-Ramírez, J.; *Catal. Today* **2014**, *235*, 176.
- Ballotin, F. C.; Perdigão, L. T.; Rezende, M. V. B.; Pandey, S. D.; da Silva, M. J.; Soares, R. R.; Freitas, J. C. C.; Teixeira, A. P. C.; Lago, R. M.; *New J. Chem.* **2019**, *43*, 2430.
- Li, X.; Shi, J.; Wang, Z.; Duan, X.; Chen, G.; Guan, Q.; Li, X.; Lei, T.; *BioResources* **2017**, *12*, 7525.
- Pasinszki, T.; Krebsz, M.; Kótai, L.; Sajó, I. E.; Homonnay, Z.; Kuzmann, E.; Kiss, L. F.; Vácz, T.; Kovács, I.; *J. Mater. Sci.* **2015**, *50*, 7353.
- de Mendonça, F. G.; Rosmaninho, M. G.; da Fonseca, P. X.; Soares, R. R.; Ardisson, J. D.; Tristão, J. C.; Lago, R. M.; *Environ. Sci. Pollut. Res.* **2017**, *24*, 6151.
- Tristão, J. C.; Oliveira, A. A. S.; Ardisson, J. D.; Dias, A.; Lago, R. M.; *Mater. Res. Bull.* **2011**, *46*, 748.
- Al Faraj, A.; Shaik, A. P.; Shaik, A. S.; *Int. J. Nanomed.* **2014**, *10*, 157.
- Dalal, M.; Greneche, J.-M.; Satpati, B.; Ghzaieel, T. B.; Mazaleyrat, F.; Ningthoujam, R. S.; Chakrabarti, P. K.; *ACS Appl. Mater. Interfaces* **2017**, *9*, 40831.
- Yu, H.; Niu, S.; Lu, C.; Li, J.; Yang, Y.; *Energy Convers. Manage.* **2016**, *126*, 488.
- Canivet, J.; Süß-Fink, G.; *Green Chem.* **2007**, *4*, 391.
- Velasco, L. F.; Maurino, V.; Laurenti, E.; Fonseca, I. M.; Lima, J. C.; Ania, C. O.; *Appl. Catal., A* **2013**, *452*, 1.
- Müller, F.; Ferreira, C. A.; Franco, L.; Puiggali, J.; Alemán, C.; Armelin, E.; *J. Phys. Chem. B* **2012**, *116*, 11767.
- Hasan, Z.; Hwang, J.-S.; Jhung, S. H.; *Catal. Commun.* **2012**, *26*, 30.
- Santos, E. M.; Teixeira, A. P. C.; da Silva, F. G.; Cibaka, T. E.; Araújo, M. H.; Oliveira, W. X. C.; Medeiros, F.; Brasil, A. N.; de Oliveira, L. S.; Lago, R. M.; *Fuel* **2015**, *150*, 408.
- Liu, T.; Li, Z.; Li, W.; Shi, C.; Wang, Y.; *Bioresour. Technol.* **2013**, *133*, 618.
- Dawodu, F. A.; Ayodele, O.; Xin, J.; Zhang, S.; Yan, D.; *Appl. Energy* **2014**, *114*, 819.
- Mar, W. W.; Somsook, E.; *Procedia Eng.* **2012**, *32*, 212.
- Brand, R. A.; *Nucl. Instrum. Methods Phys. Res., Sect. B* **1987**, *28*, 398.
- Ngaosuwan, K.; Goodwin, J. G.; Prasertdham, P.; *Renewable Energy* **2016**, *86*, 262.
- Li, H.; Wang, Y.; Zhu, Y.; Xu, X.; Wu, A.; Deng, X.; *BioResources* **2018**, *13*, 6221.
- Chen, T.; Peng, L.; Yu, X.; He, L.; *Fuel* **2018**, *219*, 344.
- Zhou, Y.; Niu, S.; Li, J.; *Energy Convers. Manage.* **2016**, *114*, 188.
- Ibrahim, N. A.; Rashid, U.; Taufiq-Yap, Y. H.; Yaw, T. C. S.; Ismail, I.; *Energy Convers. Manage.* **2019**, *195*, 480.
- Zhang, H.; Luo, X.; Shi, K.; Wu, T.; He, F.; Yang, H.; Zhang, S.; Peng, C.; *Carbon* **2019**, *147*, 134.
- Meshkani, F.; Rezaei, M.; *Chem. Eng. Res. Des.* **2015**, *95*, 288.
- Liu, W.-J.; Tian, K.; Jiang, H.; Yu, H.-Q.; *Sci. Rep.* **2013**, *3*, 2419.
- Cuesta, A.; Dhamelincourt, P.; Laureyns, J.; *Carbon* **1994**, *32*, 1523.
- Del Río, J. C.; Gutiérrez, A.; Romero, J.; Martínez, M. J.; Martínez, A. T.; *J. Anal. Appl. Pyrolysis* **2001**, *58-59*, 425.
- Branca, C.; Giudicianni, P.; Di Blasi, C.; *Ind. Eng. Chem. Res.* **2003**, *42*, 3190.
- Yu, H.; Niu, S.; Lu, C.; Li, J.; Yang, Y.; *Fuel* **2017**, *208*, 101.

45. Wieczorek-Ciurowa, K.; Kozak, A. J.; *J. Therm. Anal. Calorim.* **1999**, *58*, 647.
46. Yu, M.; Zhong, C.; Zhang, Y.; Chen, Q.; Ao, X.; Lei, X.; Li, C.; *J. Anal. Appl. Pyrolysis* **2018**, *134*, 293.
47. Hara, M.; Yoshida, T.; Takagaki, A.; Takata, T.; Kondo, J. N.; Hayashi, S.; Domen, K.; *Angew. Chem., Int. Ed.* **2004**, *43*, 2955.
48. Kastner, J. R.; Miller, J.; Geller, D. P.; Locklin, J.; Keith, L. H.; Johnson, T.; *Catal. Today* **2012**, *190*, 122.
49. Takagaki, A.; Toda, M.; Okamura, M.; Kondo, J. N.; Hayashi, S.; Domen, K.; Hara, M.; *Catal. Today* **2006**, *116*, 157.
50. Lou, W.-Y.; Zong, M.-H.; Duan, Z.-Q.; *Bioresour. Technol.* **2008**, *99*, 8752.
51. Araujo, R. O.; Chaar, J. S.; Queiroz, L. S.; da Rocha Filho, G. N.; da Costa, C.; da Silva, E. F.; Landers, G. C. T.; Costa, R.; Costa, M. J. F.; Gonçalves, A. A. S.; de Souza, L. K. C.; *Energy Convers. Manage.* **2019**, *196*, 821.
52. Neeli, S. T.; Ramsurn, H.; *Carbon* **2018**, *134*, 480.
53. Kumar, U.; Maroufi, S.; Rajarao, R.; Mayyas, M.; Mansuri, I.; Joshi, R. K.; Sahajwalla, V.; *J. Cleaner Prod.* **2017**, *158*, 218.
54. Fraga, A. C.; Quitete, C. P. B.; Ximenes, V. L.; Sousa-Aguiar, E. F.; Fonseca, I. M.; Rego, A. M. B.; *J. Mol. Catal. A: Chem.* **2016**, *422*, 248.
55. Saravanan, K.; Tyagi, B.; Shukla, R. S.; Bajaj, H. C.; *Appl. Catal., B* **2015**, *172-173*, 108.
56. Li, J.; Liang, X.; *Energy Convers. Manage.* **2017**, *141*, 126.

Submitted: January 22, 2020

Published online: March 30, 2020

